Nanotechnology

PAPER

Controlled fabrication of gold nanotip arrays by nanomolding-necking technology

To cite this article: Guoxing Han *et al* 2020 *Nanotechnology* **31** 144001

IOP Publishing Nanotechnology
Nanotechnology 31 (2020) 144001 (7pp) https://doi.org/10.1088/1361-6528/ab62cb

Controlled fabrication of gold nanotip arrays by nanomolding-necking technology

Guoxing Han[1], Yupeng Wu[1], Weidong Yan[1], Langquan Shui[1], Xiangzheng Jia[1], Enlai Gao[1,5], Minqiang Jiang[2,3] and Ze Liu[1,2,4,5]

[1] Department of Engineering Mechanics, School of Civil Engineering, Wuhan University, Wuhan, Hubei 430072, People's Republic of China
[2] State Key Laboratory of Nonlinear Mechanics, Institute of Mechanics, Chinese Academy of Sciences, Beijing 100190, People's Republic of China
[3] School of Engineering Science, University of Chinese Academy of Sciences, Beijing 101408, People's Republic of China
[4] Key Laboratory of Safety for Geotechnical and Structural Engineering of Hubei Province, School of Civil Engineering, Wuhan University, Wuhan, 430072, People's Republic of China

E-mail: enlaigao@whu.edu.cn and ze.liu@whu.edu.cn

Received 11 August 2019, revised 13 November 2019
Accepted for publication 17 December 2019
Published 17 January 2020

Abstract

The fabrication of nanotips has been driven by the increasing industrial demands in developing high-performance multifunctional nanodevices. In this work, we proposed a controlled, rapid as well as low cost nanomolding-necking technology to fabricate gold nanotips arrays. The geometries of gold nanotips having cone angle range of ~28–77° and curvature radii of <5 nm can be prepared by tailoring the diameters of raw nanorods in nanomolding process or modulating the necking temperature. Molecular dynamics simulation reveals that the formation of the nanotip geometry is determined by the interplay between dislocation-based and diffusion-based deformation mechanisms, intrinsically arising from the nonlinear dependence of atom diffusion on temperature and sample size. The good controllability, mass production and low cost of the developed nanomolding-necking technology make it highly promising in developing nanodevices for a wide range of applications, such as probing, sensing, antireflection coating and nanoindentation.

Keywords: nanomolding, necking, nanotips, deformation

(Some figures may appear in colour only in the online journal)

1. Introduction

Metal nanomaterials can be divided into zero-, one-, or two-dimensional (0, 1, 2D) structures. 1D nanostructures, consisting of rods, wires, tips, ribbons, and pores, possess fantastic properties benefiting from their quite unique structures, which make them promising for a large number of applications, such as electronic circuits, nanostencil lithography, reinforcement phase of composites, biological and chemical sensors [1]. For example, Deng *et al* recently developed controllable methods of wet etching to fabricate nanopore arrays with tunable shapes for nanostencil lithography [2, 3]. Nanotip, as one of the most intriguing members of 1D nanostructures, has been widely used in cold cathode field emission [4], scanning probe microscopy [5], antireflection coating [6] and nanoindentation [7]. To this end, considerable efforts have been made in developing nanotip fabrication technologies, which can be divided into top-down and bottom-up strategies [8], such as etching techniques [2, 3], electron deposition [9], laser ablation [10], physical vapor deposition [11], chemical vapor deposition [12], electron cyclotron resonance plasma process [13] etc. However, these methods are usually limited for mass production by their poor-controllability, complex processes or high cost. Therefore, a controlled, rapid, and low-cost nanotips fabrication technology is still highly desirable.

Necking, in engineering or materials science, refers to a tensile deformation mode of ductile materials where relatively large amounts of strain localize in a small region [14]. As a

[5] Authors to whom any correspondence should be addressed.

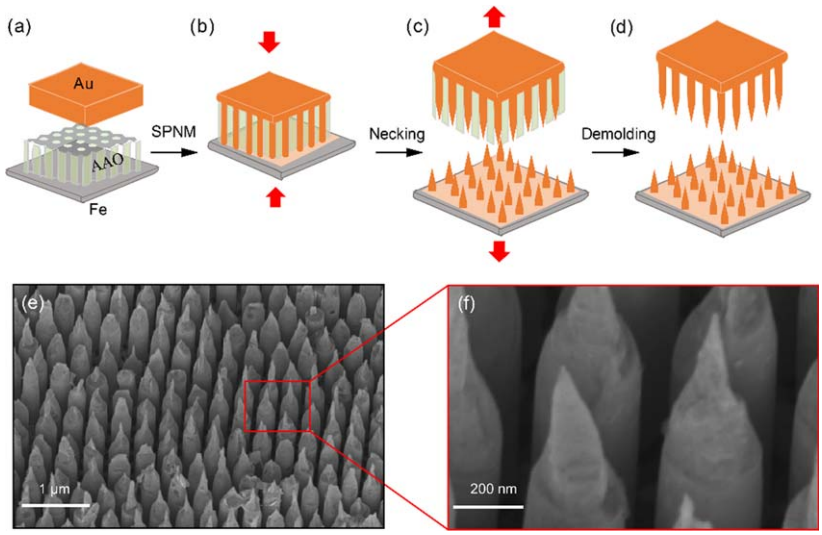

Figure 1. (a)–(d) Schematic illustration of nanomolding-necking technology. (e) Typical SEM images of gold nanotips arrays. These nanotips were obtained by necking 260 nm diameter gold nanorod array at 300 K. (f) Magnified SEM image of the selected area in (e).

common deformation and failure of material, necking has been widely used in the deformation control of rigid plastics [15, 16], large deformation of polypropylene [17–20], fabrication of glass wire or tube [21] and metallic glasses [22, 23], and preparation of high quality semiconductor metals [24]. However, the necking phenomenon has been rarely used in nanofabrication considering the challenging of manipulating small-scale specimens. Recently we demonstrate a low-cost fabrication technology of nanorods arrays, named as superplastic nanomolding (SPNM), which can fabricate nanorods arrays through either dislocation slip or atom diffusion mechanisms [25–27]. The advantage of this SPNM technology is that nanorods arrays with varying diameters can be fabricated with excellent controllability.

Combing the fabrication of nanorods arrays by SPNM and the subsequently shaping nanorods into nanotips by necking deformation, this work proposes a new strategy to fabricate gold nanotips arrays. It is found experimentally that lower-temperature necking of nanorods with larger diameters facilitates the formation of sharper nanotips. The effects of sample size and necking temperature were systematically investigated by molecular dynamics (MD) simulations, which accords with the experiments and reveals that the nanotips geometries are determined by the competition between dislocation-based and diffusion-based deformations.

2. Materials and methods

2.1. Fabrication of nanorods arrays by SPNM

The fabrication of gold nanotips arrays consists of two steps, SPNM of nanorods arrays and necking of the nanorods into nanotips, as illustrated in figures 1(a)–(d). In the first step, stainless steel thin plate, ultra-thin anodic aluminum oxide template (AAO template, produced by Shenzhen Topological Seminal Membrane Technology Company) and gold plate (purity of 99.999%, purchased from Hezheng New Material Company) were stacked as sandwich structures (figure 1(a)). The sandwich sample was put between two parallel plates of a universal testing machine, which was equipped with a home-built heater. When the sample was heated to a typical target temperature of 800 K, the metal/mold combination was compressed at a loading rate of 0.5 mm min^{-1} (corresponding to a strain rate of 8×10^{-3} s^{-1}) until 500 MPa, and then held for 600 s. The gold will fill into the AAO nanoholes through diffusion dominated creep deformation [25]. After fully filled into the AAO template, the gold nanorods will continuously grow to contact the stainless steel thin plate, and finally bond with the stainless steel through atom diffusion (figure 1(b)). Thus, gold nanorods arrays with two ends fixed onto gold and stainless steel substrate, respectively, were obtained.

AAO templates with the same diameter (~10 mm) but different through-holes having diameters of about 25 nm, 90 nm, 260 nm, and heights of 120 nm, 400 nm, 1200 nm, respectively, were used in the experiments. Therefore, the thickness of AAO template equals to the height of through-holes therein. In our experiments, the effective nanomolding region is about 3 mm in diameter, in which the pulling-off force is about 80 N (figure S1). The necking region is determined by the molded region. In principle, the gold nanotips could be uniform over large area (figure S2 is available online at stacks.iop.org/NANO/31/144001/mmedia). Because the fixing condition is very important in the fabricating of high-quality nanotips. Herein, we built a structure to clamp the stainless steel plate (with size much larger than the molded region), the induced in-plane stretching stress can thus help to reduce the out-of-plane deformation of the stainless steel plate (figure S3). In this structure, the top end of the gold rod is clamped and fixed, the stacked AAO and stainless steel plate are fixed between an orifice plate and a solid plate by using bolts (figure S3(b)).

2.2. Fabrication of nanotips by necking of the gold nanorods arrays

In the second step, the fabricated gold nanorods arrays were cooled down to various of temperatures, and subsequently the as-formed sandwich structure was stretched along the axial direction of the nanorods by oppositely pulling the gold and stainless steel substrate. The loading rate was 0.5 mm min^{-1} (strain rate of 8×10^{-3} s^{-1}). As the loading force increasing, the nanorods arrays were firstly elastically stretched, then plastically deformed and finally necked to break, which formed gold nanotips arrays (figure 1(c)). The produced structure was then immersed in a KOH solution (with concentration of 3 mol l^{-1} and temperature of 300 K) for 2 h to remove the AAO template, the gold nanotips arrays attached on the surface of the gold and stainless steel substrates were obtained (figure 1(d)).

2.3. Measurement of nanotips geometries

To accurately characterize the geometries of the prepared gold nanotips, two generatrixes of the circular truncated cone were extended to intersect in a single point, and the angle between these lines is defined as the cone angle of a nanotip. Specifically, we use a field emission scanning electron microscopy (SEM, Zeiss Sigma 500) to measure the cone angle of the nanotips. The prepared sample was placed onto the sample stage of the SEM. The sample stage was tilted by 60° to get a good view of the nanotips. Since the gold nanotips are perpendicular to the gold substrate and hence the sample stage, the angle between the electron beam and the nanotips will be also 60°. Therefore, the actual cone angle of a nanotip (α) can be calculated based on the observed cone angle (β) by the geometric conversion [26, 28]

$$\alpha/2 = \tan^{-1}\left(\frac{\sqrt{3}}{2}\tan\beta/2\right). \quad (1)$$

2.4. MD simulation

MD simulations were carried out using large-scale atomic/molecular massively parallel simulator computational package [29]. The optimized embedded atom method potential is adopted for its high fidelity and robustness [30]. The Newton equations of motion are integrated using the Verlet algorithm with a time step of 1 fs. Circular-cross-section gold nanorods were created out of an ideal centered cubic crystal with cross-section orientations of [100]. All the samples are modeled with length of 50 nm but varying diameters from 6 to 10 nm. Before the tensile deformation protocol, the prepared samples were first fully relaxed to an equilibrium configuration using a conjugated-gradient algorithm and then thermally equilibrated to target temperatures (300 and 800 K) for 100 ps using a Nosé–Hoover thermostat with a characteristic relaxation time of 0.1 ps. Afterwards, the uniaxial tensile strain with a strain rate of 3×10^{7} s^{-1} was applied by deforming the periodic simulation box along axial direction until failure of structures. Finally, the formed nanotips were equilibrated at the target temperatures for 100 ps to track their morphology evolution.

3. Results and discussion

3.1. Characterization of the prepared gold nanotips by nanomolding-necking technology

Figures 1(e), (f) show a typical morphology of the prepared gold nanotips arrays characterized by SEM. A gold rod with diameter of 3 mm and height of 1 cm was stacked between a 10 mm diameter AAO template, which has nanoholes with diameter of 260 nm and height of 1200 nm, and a stainless steel plate with thickness of 50 μm. The processing conditions for nanomolding and necking are described in the materials and methods section. Because of the constraints between nanorods and AAO template during the stretching process, the necking region of nanorods usually occurs near the roots of the nanorods. Thus the average height of the nanotips arrays is equal to the thickness of AAO template and generally uniform. The necking randomly occurs nearing the roots of nanorods, which can be attributed to the stress concentration at the roots for the nucleation of necking. It should be noted that the shapes of gold nanotips on both the stainless steel substrate and gold substrate are observed similar (figure S4). Additionally, high-aspect-ratio tips called 'rocket tips' [31] can be prepared by simply using AAO templates with high-aspect-ratio nanopores in our method. The uniformity of the prepared gold nanotips arrays on a large scale (figure 1(e)) indicates the high efficiency and mass production of our method. Especially, by zooming-in the nanotips (figure 1(f)), it is amazing to find that the curvature radii of the nanotips were smaller than 5 nm. Such a sharp tip is highly desirable for the applications in tip-enhanced sensors as well as high-resolution imaging in scanning probe microscopy.

3.2. Modulating the geometries of nanotips by necking nanorods with different diameters

The properties of nanorods are highly related to their specific surface area [32]. To investigate the surface effect on the nanotips geometries, we used 10 mm diameter AAO templates having through-holes with diameters of 25 nm, 90 nm, 260 nm, and heights of 120 nm, 400 nm, 1200 nm, respectively, from which nanorods with different diameters were prepared by SPNM. After necking the nanorods arrays at 300 K (see materials and methods section for details), gold nanotips arrays with different geometries were prepared (figures 2(a)–(c)), where the cone angles of the nanotips were measured and calculated by using equation (1) as 62°, 53° and 34° for the nanorods with diameter of 22, 86 and 260 nm, respectively. By measuring at least 10 nanotips for each size, the averaged parameters of nanotip geometries were obtained. It is clear that as the diameters of nanorods increased from 25 ± 3 nm, 90 ± 5 nm to 268 ± 28 nm, the cone angle decreases from $62 \pm 7°$, $50 \pm 3°$ to $31 \pm 5°$, respectively. We can herein conclude that the larger nanorod diameter will result in the sharper nanotips. By further comparing the morphologies of the nanotips fabricated from nanorods with varying diameters, we observed that the length of necking zone increases with the increasing of diameter of nanorods

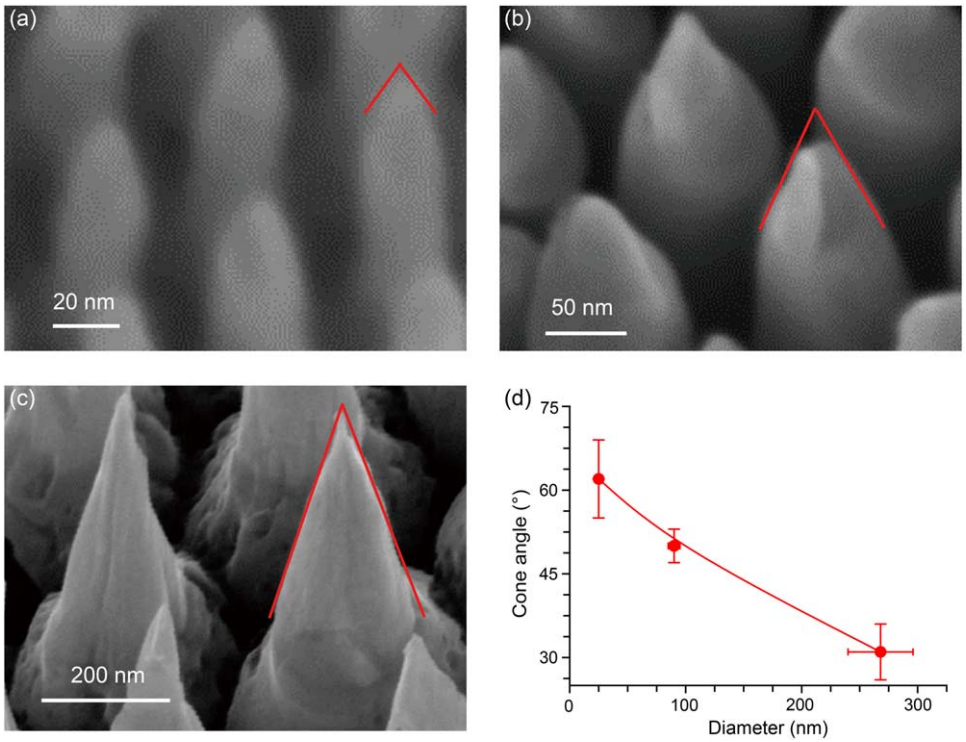

Figure 2. SEM images of the fabricated nanotips having diameters of (a) 22 nm, (b) 86 nm, and (c) 260 nm. (d) The relationship between the cone angles and the diameters of nanorods.

(figures 2(a)–(c)). However, it is noted that the curvature radii of the nanotips are almost insensitive to the diameters of the nanorods under these conditions, which are less than 5 nm for all the samples (figures 2(a)–(c)).

3.3. Modulating the geometries of nanotips by controlling the necking temperatures

To investigate the temperature effect on the geometries of gold nanotips, the necking of gold nanorods arrays was carried out at different temperatures. To avoid the coupling with the effect of nanorod size as investigated above, the AAO template with the same diameter of 260 nm was used, while three necking temperatures (300, 500 and 800 K) were chosen. The fabricated nanotips are shown in figures 3(a)–(c). Again, we measured and calculated the cone angles of the nanotips and the results are summarized in figure 3(d). We observed that the lower necking temperature leads to the sharper nanotips. Specifically, the cone angles of nanotips prepared at 300 K, 500 K, and 800 K are 28 $\pm$ 5°, 62 $\pm$ 7° to 77 $\pm$ 5°, respectively (figure 3(d)), indicating the wide tunability of nanotip geometries by modulating necking temperature.

3.4. Mechanism discussions

To understand the underlying mechanism of the observed influence of nanorod diameters and necking temperatures on the sharpness of nanotips, MD simulations of nanorods with different diameters stretched at varying temperatures were conducted (see materials and methods section for details). The results are summarized in figure 4. It can be found that the nanorods experience clearly necking process and thus develop into atom-thick nanotips. The geometries of gold nanorods with larger diameter evaluated more gently in wide regions and thus formed sharper nanotips. Meanwhile, the tips become blunt with the increasing of processing temperature. This evolution trend of nanotips modulated by sample size and processing temperature agrees well with our experimental observation, which can be explained by the interplay between dislocation and atom diffusion-based deformations. The dislocation-dominated deformation in the necking (strain localization) process is critical to create atomic steps and thus form sharp nanotips, while the diffusion helps to smooth out atomic steps in the tip surface and thus reduce the sharpness of nanotips. The diffusion coefficient for the atom diffusion can be given as

$$D \propto \nu e^{-\Delta E/k_{\mathrm{B}}T}, \tag{2}$$

where ν and ΔE are the vibrational frequency of atoms and the potential energy barrier to diffusion, respectively, T is temperature, and k_{B} is the Boltzmann constant. As shown in figure 4, the potential energy of surface atoms is generally higher than that of bulk atoms, indicating their high activity (low ΔE) that leads to fast atom diffusion (high D). The specific area in nanorods with smaller diameters is larger, making the diffusion-based deformation mode arises and thus blunting the tips. Similarly, the increasing of processing temperature (high $k_{\mathrm{B}}T$) will also induce fast atom diffusion (high D) and thus blunt the tips. In general, as the nanorods have small diameters or are processed at high temperature, the gold atoms at the surface, especially at the

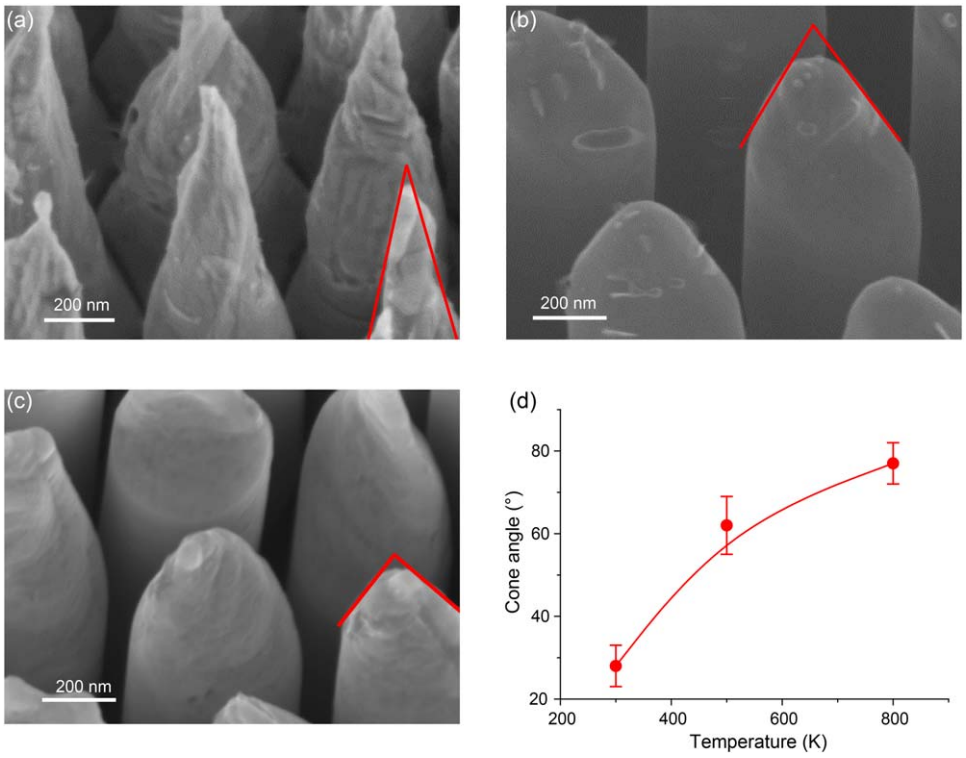

Figure 3. SEM images of nanotips obtained by necking 260 nm diameter nanorods at temperatures of (a) 300 K, (b) 500 K and (c) 800 K. (d) The relationship between the cone angle and the processing temperature.

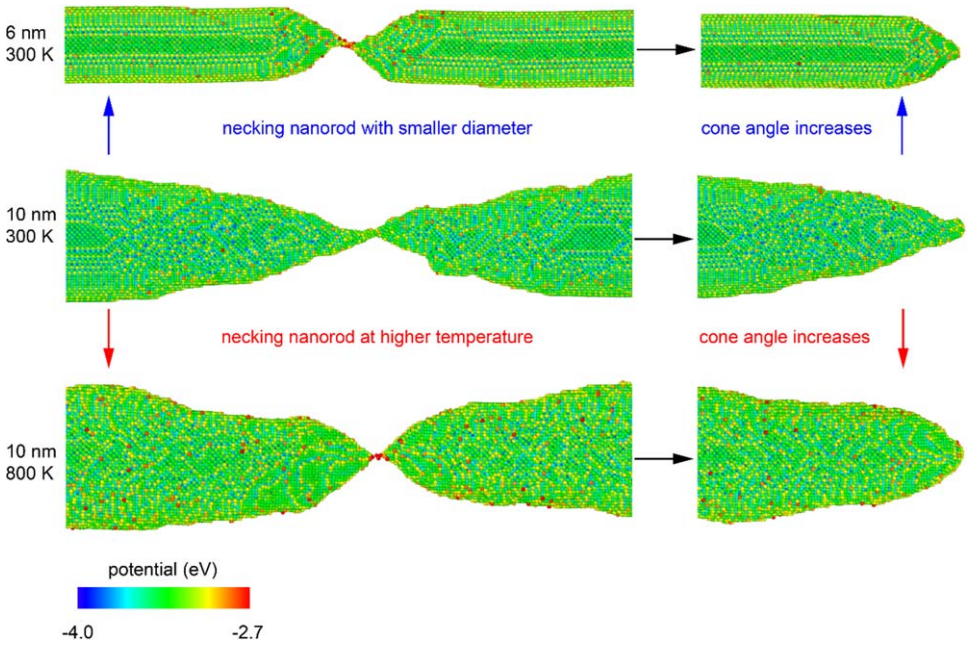

Figure 4. Snapshots of the nanorods having varying diameters (6 and 10 nm) stretched at different temperatures (300 and 800 K) before breaking and after breaking with equilibrium time of 100 ps. Atoms are colored by their values of potential energy.

top surface of nanotips diffuse easily towards the base of nanotips to minimize the system energy, and thus form nanotips with large cone angles. Otherwise, as the dislocation-based deformation dominates the formation of nanotip geometries, the continuous dislocation slip is apt to render the sharp tips (figure 4).

As discussed previously, the curvature radii of nanotips can be affected by the necking temperature and the specific area of samples. In addition, the uniformity of the prepared nanotips arrays highly affects its wide applications. To solve this problem, ordered AAO templates with good uniformity should be used for fabricating uniform nanorods. Fortunately, there are some

literatures reporting the preparation of uniform AAO templates by adding a pre-stamping process [33, 34]. In addition to improving the uniformity of nanorods, the necking of nanorods also influences the top shape and height of each nanotip, which closely relates to the necking temperature and defects of nanorods. Although elevating the necking temperature can improve the uniformity, the curvature of the top shape becomes larger because of the fast atom diffusion. Thus to improve the uniformity of nanotips, future efforts should be directed, but not limited, at fabricating defect-controlled nanorods and necking the nanorods under proper processing conditions.

Additionally, we remark here that there are some limits on MD simulations. The strain rate ($3 \times 10^7 s^{-1}$) in the simulations is much higher than that used in experiments (8×10^{-3} s^{-1}). The high strain rate is expected to reduce the time for atom diffusion in the necking and thus helps to form sharper nanotips, which results in some discrepancies between the MD simulations and the experiments. For example, the cone angle of 10 nm diameter nanotips observed in simulation is 30° (necking at 300 K, figure 4), while the cone angle of 22 nm diameter nanotips prepared at 300 K from experiments is much larger (62°, figure 2(a)). Despite these discrepancies, the MD simulations captured the evolution trend of nanotip morphologies that are modulated by the effects of surface and temperature on atom diffusion, which agrees well with the experimental observations.

4. Conclusion

In summary, based on the developed nanomolding-necking technology, gold nanotips with controlled cone angles (from 28° to 77°) and extremely small curvature radii (<5 nm) were fabricated. It is found that the nanorod diameter and the necking temperature play important roles in the shaping of nanotips. By using MD simulations, the underlying mechanism is revealed as the competition between atom diffusion and dislocation based deformation mechanisms. These findings not only pave a way to study the deformation mechanism in metal nanorods, but also provide a practical technology for the mass fabrication of metal nanotips with strong controllability, easy scalability as well as low cost.

Acknowledgments

This work was supported by the Opening fund of State Key Laboratory of Nonlinear Mechanics, the National Natural Science Foundation of China (11902225, 11872284, 11632009, and 11602175), Wuhan Science and Technology Bureau (2019010701011390), and the Fundamental Research Funds for the Central Universities (413000091).

ORCID iDs

Langquan Shui https://orcid.org/0000-0002-5079-9629
Enlai Gao https://orcid.org/0000-0003-1960-0260
Ze Liu https://orcid.org/0000-0002-9906-5351

References

[1] Xia Y, Yang P, Sun Y, Wu Y, Mayers B, Gates B, Yin Y, Kim F and Yan H 2003 One-dimensional nanostructures: synthesis, characterization, and applications *Adv. Mater.* **15** 353–89
[2] Deng T, Wang Y F, Chen Q, Chen H J and Liu Z W 2016 Massive fabrication of silicon nanopore arrays with tunable shapes *Appl. Surf. Sci.* **390** 681–8
[3] Deng T, Li M W, Chen J, Wang Y F and Liu Z W 2014 Controllable fabrication of pyramidal silicon nanopore arrays and nanoslits for nanostencil lithography *J. Phys. Chem.* C **118** 18110–5
[4] Houdellier F, Masseboeuf A, Monthioux M and Hytch M J 2012 New carbon cone nanotip for use in a highly coherent cold field emission electron microscope *Carbon* **50** 2037–44
[5] Rezeq M d and Joachim C 2010 *Scanning Probe Microscopy* (Singapore: World Scientific)
[6] Southwell W H 1991 Pyramid-array surface-relief structures producing antireflection index matching on optical-surfaces *J. Opt. Soc. Am.* A **8** 549–53
[7] Kumaravelu G, Alkaisi M M, Bittar A, Macdonald D and Zhao J 2004 Damage studies in dry etched textured silicon surfaces *Curr. Appl Phys.* **4** 108–10
[8] Chattopadhyay S, Chen L and Chen K 2006 Nanotips: growth, model, and applications *Crit. Rev. Solid State Mater. Sci.* **31** 15–53
[9] Belova L M, Hellwig O, Dobisz E and Dan Dahlberg E 2012 Rapid preparation of electron beam induced deposition Co magnetic force microscopy tips with 10 nm spatial resolution *Rev. Sci. Instrum.* **83** 093711
[10] Pedraza A J, Fowlkes J D and Lowndes D H 1999 Silicon microcolumn arrays grown by nanosecond pulsed-excimer laser irradiation *Appl. Phys. Lett.* **74** 2322–4
[11] Wu Z S, Deng S Z, Xu N S, Chen J, Zhou J and Chen J 2002 Needle-shaped silicon carbide nanowires: synthesis and field electron emission properties *Appl. Phys. Lett.* **80** 3829–31
[12] Babu E S, Saravanakumar B, Ravi G, Yuvakkumar R, Ganesh V, Guduru R K and Kim S 2018 Zinc oxide nanotips growth by controlling vapor deposition on substrates *J. Mater. Scie.—Mater. Electron.* **29** 6149–56
[13] Hsu C H, Lo H C, Chen C F, Wu C T, Hwang J S, Das D, Tsai J, Chen L C and Chen K H 2004 Generally applicable self-masked dry etching technique for nanotip array fabrication *Nano Lett.* **4** 471–5
[14] Bridgman P W 1952 *Studies in Large Plastic Flow and Fracture* (New York: McGraw-Hill)
[15] Vincent P I 1960 The necking and cold-drawing of rigid plastics *Polymer* **1** 7–19
[16] Georgievskii D 2015 Uniaxial extension of a thin rigid-plastic sheet in the presence of a neck *Dokl. Phys.* **60** 310–3
[17] Sweeney J, Collins T L D, Coates P D and Ward I M 1997 Application of an elastic model to the large deformation, high temperature stretching of polypropylene *Polymer* **38** 5991–9
[18] Ibhadon A O 1990 Neck profiles in drawn polypropylene and ethylene propylene copolymers *Makromolekulare Chem.—Macromol. Chem. Phys.* **191** 1375–82
[19] Liu T and Harrison I R 1987 The temperature rise on neck formation of polymers: polypropylene and polyethylene *Polymer* **28** 1860–2
[20] Taylor W N and Clark E S 1978 Superdrawn filaments of polypropylene *Polym. Eng. Sci.* **18** 518–26
[21] Takayama S 1981 Fabrication of metallic-glass wire or tube by drawing *J. Mater. Sci.* **16** 269–71
[22] Hu Z, Meduri C S, Blawzdziewicz J and Kumar G 2019 Nanoshaping of glass forming metallic liquids by stretching: evading lithography *Nanotechnology* **30** 075302

[23] Hasan M and Kumar G 2017 High-throughput drawing and testing of metallic glass nanostructures *Nanoscale* **9** 3261–8
[24] Langdo T A, Leitz C W, Currie M T, Fitzgerald E A, Lochtefeld A and Antoniadis D A 2000 High quality Ge on Si by epitaxial necking *Appl. Phys. Lett.* **76** 3700–2
[25] Liu Z 2017 One-step fabrication of crystalline metal nanostructures by direct nanoimprinting below melting temperatures *Nat. Commun.* **8** 14910
[26] Liu Z, Han G, Sohn S, Liu N and Schroers J 2019 Nanomolding of crystalline metals: the smaller the easier *Phys. Rev. Lett.* **122** 036101
[27] Liu Z 2019 Investigation of temperature and feature size effects on deformation of metals by superplastic nanomolding *Phys. Rev. Lett.* **122** 016101
[28] Rose D J 1956 On the magnification and resolution of the field emission electron microscope *J. Appl. Phys.* **27** 215–20
[29] Plimpton S 1995 Fast parallel algorithms for short-range molecular-dynamics *J. Comput. Phys.* **117** 1–19
[30] Sheng H W, Kramer M J, Cadien A, Fujita T and Chen M W 2011 Highly optimized embedded-atom-method potentials for fourteen FCC metals *Phys. Rev.* B **83** 134118
[31] Boisen A, Hansen O and Bouwstra S 1996 AFM probes with directly fabricated tips *J. Micromech. Microeng.* **6** 58–62
[32] Park H S and Zimmerman J A 2005 Modeling inelasticity and failure in gold nanowires *Phys. Rev.* B **72** 054106
[33] Li J J, Zhang W W, Song Y J, Yin W T and Zhang T 2016 Template transfer nanoimprint for uniform nanopores and nanopoles *J. Nanomater.* **2016** 1–7
[34] Alam K M, Singh A P, Bodepudi S C and Pramanik S 2011 Fabrication of hexagonally ordered nanopores in anodic alumina: an alternative pretreatment *Surf. Sci.* **605** 441–9